CrossMark

ORIGINAL PAPER

Rheology of microfibrillated cellulose (MFC) suspensions: influence of the degree of fibrillation and residual fibre content on flow and viscoelastic properties

Michel Schenker · Joachim Schoelkopf · Patrick Gane · Patrice Mangin

Abstract The influence of the degree of fibrillation (*DoF*), i.e. the fibril width distribution, on the rheological properties of microfibrilated cellulose (MFC) suspensions was investigated. To extend the understanding of the dominating effect of either fibril diameter alone or diameter size distribution, flow curves (viscosity against shear rate) and viscoelastic measurements were performed on single, double and ternary component mixtures of medium and highly fibrillated MFCs and pulp fibres across a range of solids content. The data were quantified using classical and recently introduced descriptors, and presented in comprehensive 3D/ternary contour plots to identify qualitative trends. It was found that several rheological properties followed the trends that are generally described in the literature, i.e. that an increasing DoF increases the MFC suspension network strength. It was, however, also found that coarse pulp fibres can have additional effects that cannot be explained by the increased fibril widths alone. It is hypothesised that the increased stiffness (directly caused by the larger fibril width) as well as the reduced mobility of the pulp fibres are additional contributors. The data are discussed in relation to recent findings in the field of rheology and related morphological models of MFC suspension flow behaviour.

M. Schenker (✉) · P. Mangin
University of Quebec in Three Rivers (UQTR), 3350 Boulevard des Forges, Trois-Rivières, QC G9H 5H7, Canada
e-mail: michel.schenker@fiberlean.com

P. Mangin
e-mail: patrice.mangin@uqtr.ca

M. Schenker
FiberLean Technologies Ltd., Par Moor Centre, Par Moor Road, Par, Cornwall PL24 2SQ, England, UK

M. Schenker · J. Schoelkopf · P. Gane
Omya International AG, Baslerstrasse 42, 4665 Oftringen, Switzerland
e-mail: joachim.schoelkopf@omya.com

P. Gane
e-mail: patrick.gane@omya.com

P. Gane
Department of Bioproducts and Biosystems, School of Chemical Engineering, Aalto University, 00076 Aalto, Helsinki, Finland

Graphical abstract
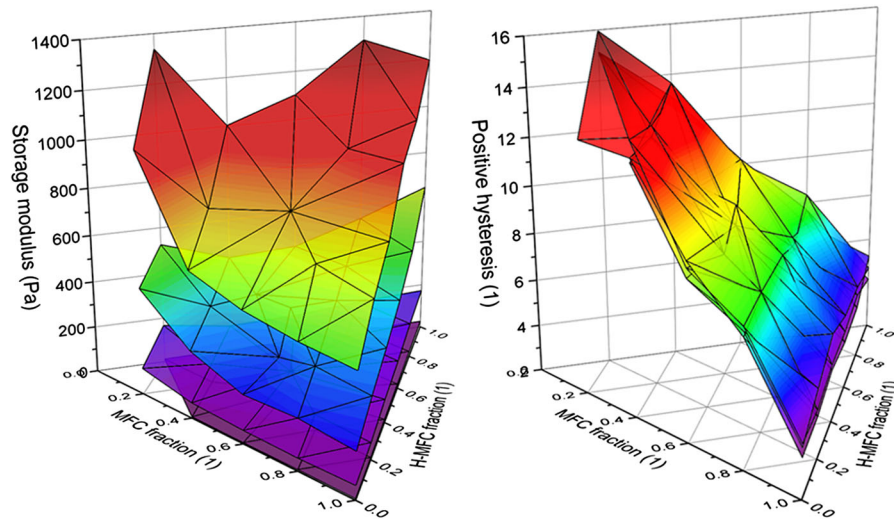
Introduction

The nanocellulose (NC) material-space contains a wide variety of different products with unique properties, despite their same underlying chemistry. The grades are ranging from fibrillated over crystalline to bacterial cellulose, and they have characteristic widths in the micrometre as well as in the nanometre range, they have medium to very high aspect ratios and can be manufactured from very different source materials (Nechyporchuk et al. 2016a). Chemical modifications of the surface hydroxyl groups widen the property- and application-space even more (Missoum et al. 2013; Stenstad et al. 2008). The classification of such a versatile material class is challenging, and still not completely aligned. Yet, a common strategy is to differentiate between bacterial, fibrillated and crystalline grades. Within the latter two, another classification regarding their characteristic size, i.e. fibril diameter or width for fibrillated grades, or crystallite size (width and length), is applied (Kangas et al. 2014). Typical examples of fibrillated grades are microfibrillated cellulose (MFC) or nanofibrillated cellulose (NFC), both of which having different names

like cellulose filaments (CF) or cellulose nanofibrils (CNF).

Due to their chemistry, but also due to their shape and mechanical properties, fibrillated cellulose materials yield high viscous aqueous suspensions, already at low solids contents (Herrick et al. 1983; Pääkkö et al. 2007). The ability of the fibrils to form networks and aggregates, to entangle and to align, as well as their flexibility leads to a complex rheological behaviour (Hubbe et al. 2017). The same applies for crystalline cellulose suspensions, where the typically platelet shaped crystallites can organise in different phases, and, due to their crystalline nature, specifically interact with visible light (Shafiei-Sabet et al. 2012). There seems to be an increasing interest, not only in NC materials in general, but also in investigating their complex aqueous suspension rheology, as is apparent, for example, from two recent review articles in the field (Hubbe et al. 2017; Nechyporchuk et al. 2016b). On the one hand, it is necessary to know the rheology of these materials in practical applications, e.g. during pumping, extrusion or casting processes to make them processable. On the other hand, an understanding of the rheology with respect to the underlying suspension particulate morphology and chemistry enables researchers to design products for very specific needs.

A major challenge in MFC rheology measurements is the non-linear behaviour, and the heterogeneous, at least two-phase, composition. Related effects include complete or partial phase-segregation (depleted, water

rich layers or voids), related apparent wall slip, and shear banding (Haavisto et al. 2015; Nazari et al. 2016; Nechyporchuk et al. 2014). The presence and the intensity of such effects do not only depend on the shear conditions, but also on the measurement system and protocol (Schenker et al. 2017). Not taking such effects into account, may lead to contradictory results, not infrequent in the literature, and probably wrong model hypotheses. Quite some effort is put into quantifying these effects (Yoshimura and Prud'-homme 1988), mathematically correcting them (Mohtaschemi et al. 2014a, b), and in developing protocols on how to avoid or supress them (Barnes 2000). Cloitre and Bonnecaze (2017) pointed out in a recent review on wall slip of high solids dispersions, that such mechanisms are often considered as a nuisance because they violate assumptions and boundary conditions of the measurement method, yet it should be understood, that those mechanisms are fundamental components of how the material responds to the deformation. This valid comment highlights that it is as important to be at least aware of such effects, ideally quantify and describe them, rather than trying to suppress them.

Occasionally, complementary measurement techniques are used to quantify directly or indirectly such non-linear effects, though they can also be used to study the suspension morphology under different shear conditions. Such complementary techniques include optical imaging (Saarikoski et al. 2012), velocity profiling using, e.g. ultrasound and/or tomography techniques (Kataja et al. 2017), and structural investigations like small angle neutron scattering (Orts et al. 1998) or X-ray scattering (Nechyporchuk et al. 2015). Such work has revealed, for instance, the tendency of unmodified MFC and NFC suspensions to aggregate (flocculate) at intermediate shear rates in constant shear experiments (Martoïa et al. 2015), or the presence of a water (-rich) film close to measurement boundary geometries, as well as concentration gradient development and plug flow under certain shear conditions (Kataja et al. 2017).

It is well known that various suspension and cellulose fibril/crystallite conditions have an influence on the nanocellulose suspension rheology. Prominent conditions are the suspensions solids content, pH, salinity or temperature (Agoda-Tandjawa et al. 2010; Pääkkö et al. 2007). To a lesser extent, also the influences of the fibril dimensions, aspect ratio (the

degree of fibrillation, short *DoF*) and surface charge (Besbes et al. 2011), and their respective probability and spatial distributions (Colson et al. 2016; Moberg et al. 2017), on the suspension rheology are investigated. In the case of mechanically produced (with or without enzymatic pre-treatments) MFC materials, the sign of the specific surface charge and the total surface charge is given by the feed pulp, and predominantly the *DoF* is changed during processing. Yet, processing towards increased *DoF* may still potentially change the surface charge density of the fibrils due to a potential release of solubles, hemicellulose and/or lignin from the original fibre structure into the suspension, though the process per se, being purely mechanical, does not add or subtract charge. Depending on the process and the process conditions, very different fibril width and length distributions, as well as residual fibre content may result. With a view, for example, on qualifying rheological measurements as quality control tools, or manufacturing a product with a dedicated rheology profile (rheological property profile is tailored to fit a specific application), the understanding of the influence of the *DoF* on the rheological behaviour of the suspension can be very beneficial.

The aim of this work was to investigate the influence of the DoF, including the impact of residual, coarse fibres on rheological properties of MFC suspensions. Of particular interest were industrial type of MFC suspensions, typically characterised to have a broad size distribution, i.e. containing residual fibres and nanometre sized fibrils together with the main body of micrometre sized fibrils. In contrast to other works in this area, we chose to use only mechanical fibrillation processes to obtain different *DoF* MFC suspensions in order to exclude surface charge related effects (Moberg et al. 2017). To obtain a wide variety of different *DoF*s, but without changing other aspects of the fibrils, an extensive ternary mixture trial matrix was set-up. To be able to identify potential trends, the data were quantified using previously introduced techniques and descriptors (Schenker et al. 2017, 2018). Finally, the findings are discussed phenomenologically with a view on potential suspension morphologies, based on recent models obtained from rheo-optical studies of MFC suspensions (Haavisto et al. 2015; Karppinen et al. 2012; Martoïa et al. 2015). The work presented here is intended not only to motivate other researchers in the

field to consider thorough quantification of their rheological data, but also to propose some interesting aspects to investigate further the use of optical, or other, structure revealing techniques in combination with rheological studies of MFC suspensions.

Methods

Materials

To obtain samples made up of fibrillated cellulose material having three different degrees of fibrillation (*DoF*) whilst trying to avoid changing other material characteristics, like surface chemistry and charge, only mechanical fibrillation processes of increasing intensity were applied to a starting batch of a eucalyptus pulp suspension made down in tap water from dry pulp mats. The lowest *DoF* material in this study, representing residual fibres, was the eucalyptus pulp itself, denoted as *pulp*. Respective concentrations of *pulp* suspension were manufactured by adding according amounts of dry mat pulp to water under stirring using a dissolver disc type impeller.

The manufacturing process of the intermediate *DoF* material, denoted in this work simply as *MFC*, is described in detail elsewhere (Schenker et al. 2016a) and was the same as in recent works also reported by Schenker et al. (2017, 2018). In short, the eucalyptus pulp was mechanically disintegrated at 3 wt% in tap water using an ultrafine friction grinder under a varying chosen number of single passes, each at a different rotational speed. The specific grinding energy, is defined as the total electrical energy consumption normalised by the amount of dry cellulose matter was 7.2 kW h kg^{-1}.

To achieve a higher *DoF* MFC (short *H-MFC*) an additional fibrillation process was applied to the previously described *MFC* suspension, namely an homogenisation process. To avoid having to undergo a subsequent concentration of the short *H-MFC* suspensions for the following rheological characterisation, the solids content for the homogenisation process was set to 2 wt%. This is a rather high solids content for homogenisation in laboratory scale, so, to avoid blockages or other process failures, the starting *MFC* suspension was subjected again to an ultrafine friction grinder pass at 500 min^{-1} (rpm) and a gap setting of "− 80 μm", maintaining the solids concentration still

at 3 wt%. The process was carried out on an NS 2006 L homogeniser (Niro Soavi), equipped with an LPN60 dispersion module (formerly Serendip AG, now Neztsch-Gruppe, Germany). The suspension was then subjected to single passes, with a throughput pump setting of 30 dm^3 h^{-1} and a pressure of 600 bar for all passes, achieved by adjusting the back-pressure handle accordingly. For the first ten passes, a 120 μm diameter nozzle was used to avoid clogging. To intensify the fibrillation process, an 80 μm diameter nozzle was used for two additional passes. The specific energy input of these additional process steps was 20.7 kW h kg^{-1}.

Mixtures of the three materials, *pulp*, *MFC* and *H-MFC* were realised by adding the respective amounts of the suspensions and diluting the combination by the addition of tap water. The realised dilutions were 0.5, 1, 1.5 and 2 wt% and the mixture matrix can be found in Figure 2 of the supplementary information. The mixtures, as well as the pure *MFC* and *H-MFC* suspensions were treated by 2 min of rotor stator mixing at 12,000 min^{-1} (rpm) (Polytron PT 3000, Kinematica, Switzerland) and 5 min exposure to an ultrasonic bath (Transsonic T 890, Elma, Switzerland). Before further measurements, the dilutions were let to rest for at least 1 h.

Data presentation

The rheological data are presented in ternary contour plots, one for each solids content. For a complementary visualisation, the contour surfaces are overlaid using a rainbow-type colour gradient, starting from purple at low values and ending at red for high values. The scale among the different ternary plots within one property is the same, so also the dependence on the solids content is directly visible. Instead of providing a separate colour scale, several contour lines within a ternary diagram are labelled with their respective values. A detailed introduction on the interpretation of ternary diagrams is provided in the supplementary information, but, generally speaking, the diagrams describe the composition of a ternary mixture, always adding up to 100%. Each vertex of the triangle represents 100% of one of the three components. The share of this component decreases constantly along the bisector of this vertex perpendicular to the opposite edge until it reaches that opposing side, where the share of this component is 0%. In the present work, the

left vertex represents 100% *pulp*, the right vertex 100% *MFC* and the top vertex (apex) 100% *H-MFC*. Missing data points in the ternary graph mean that the specific mixture at the respective dilution was not evaluated because it was disturbed by irreproducible or other physical effects. An example of such an effect is the observation of sedimentation after high shear under decreasing shear rate at low solids content (0.5 wt% suspensions) due to structure breakdown.

Alternatively set-up ternary diagrams can be found in the supplementary information document. Also, animated 3D ternary diagrams where the different solids content data were stacked can be found in the online repository. Each solids content dataset is represented as individual surface. The grid line colour indicates the solids content (purple: 0.5 wt%, blue: 1 wt%, green: 1.5 wt% and red: 2 wt%).

Degree of fibrillation analysis

Several attempts were made to determine the fibre and fibril width distributions of the sample materials using image analysis methods. Due to the anticipated high polydispersity of the materials, SEM-image based techniques were evaluated rather than AFM or TEM based ones in an attempt to give visual confirmation and sufficient statistical relevance. Namely, two approaches described by Onyianta and Williams (2018) and Pyrgiotakis et al. (2018) were reproduced, including modifications in the sample preparations. Unfortunately, either the obtained images were not suitable for image analysis (overlapping and confused configuration), or the obtained distribution histograms did not represent the apparent full width distributions (insufficient statistical relevance), i.e. they were not able to account for the coarser fibril/fibre fraction, like described for instance by Colson et al. (2016). Additional details on the apparent width distribution discrepancy can be found in the supplementary information. However, the exercise enabled us to identify the tendency of fibrils to aggregate at rest, even under very dilute regimes (perhaps meniscus force), as being one of the major challenges here. Common strategies to improve the level of dispersion, like adding carboxymethyl cellulose (Veen et al. 2015), were not sufficient (probably again related to the high levels of dilution).

The evolution of the degree of fibrillation (DoF) in this work is therefore indicated by qualitative and indirect data, namely by optical and scanning electron microscopy images and specific surface area (BET) measurements. For this, 0.5 wt% suspensions of pulp, *MFC* and *H-MFC* were frozen by immersion into liquid nitrogen directly after the ultrasonication step of the makedown procedure. The frozen samples were then subjected to freeze-drying (Alpha 1-2LD Freeze Dryer, Martin Christ GmbH, Germany). The specific surface area was measured using the Brunauer–Emmett–Teller (BET) method on torn out pieces of the resulting aerogels, sampled in duplicate (Tristar, Micromeritics, Germany). SEM images (Sigma VP, Zeiss, Switzerland) were taken as well from such torn-out pieces after being sputtered with gold (8 nm). For optical microscopy (Axio Imager.M2m, Zeiss, Switzerland), one drop of the respective 0.5 wt% suspension was placed between two glass slides.

Rheological measurements

All the rheological measurements were performed on an MCR 300 rheometer (Anton Paar, Austria) at 20 °C, equipped with a vane (six blades) in serrated (length profiled) cup system (vane: ST22-6V-16, d_{vane} = 22 mm, cup: CC27-SS-P, d_{cup} = 28.88 mm, profile depths = 0.5 mm, profile widths = 1.65 mm), also supplied by Anton Paar. The vane system was used because it is less prone to depletion at the wall and related apparent slip effects, as described, for example, by Mohtaschemi et al. (2014a) and Schenker et al. (2017).

All the suspensions were measured as triplicates, and each measurement within a triplicate was obtained from a separate filling of the measurement system. For a given dilution, several dilution makedowns were used throughout the work presented here, and the repeatability was checked in all cases (data not shown). The data are presented as average values from the triplicate measurements. Individual standard deviations are not presented, however, typical maximal standard deviations are provided for a given property as per cent of the average property values. Further standard deviation data can also be found in preceding work (Schenker et al. 2017, 2018). After loading the samples and immersing the vane, the system was let to rest for about 2 min before the measurement protocols were started. No pre-shearing protocol was applied in order to induce as little morphological changes to the suspension as possible.
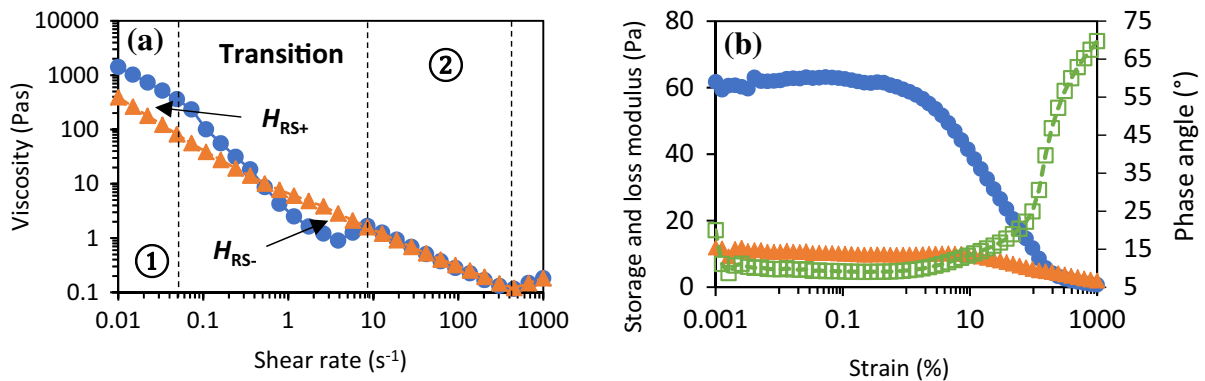
Fig. 1 Flow curve (**a**) and amplitude sweep (**b**) measurement data of a 1 wt% *MFC* suspension. In the flow curve, the blue circles represent shear rate increase data and the orange triangles represent shear rate decrease data. In the amplitude sweep graph, the blue circles and the orange triangles represent the storage and loss moduli, respectively, and the hollow squares represent the phase angle

Flow curves (viscosity η in dependence of the shear rate $\dot{\gamma}$) were recorded by performing an automated shear rate increase ramp from 0.01 to 1000 s^{-1}, directly followed by a ramp with reversed direction. 30 log-equidistant distributed point measurements were performed per ramp with automated acquisition time mode (minimal acquisition time is 15.2 s) and shear rate control. The automated acquisition time mode should ensure a steady state situation when acquiring a measurement (Schenker et al. 2016b). Having a steady state situation is important for the data interpretation with view on suspension morphology as it reduces the likelihood of time-dependent or start-up effects interferences (Puisto et al. 2015; Korhonen et al. 2017). Preliminary experiments have shown that the same flow curves can be obtained with different amounts of point measurements (data not shown). The typically obtained three region flow curve, exemplified with a 1 wt% *MFC* suspension flow curve in Fig. 1, was quantified using the descriptors introduced by Schenker et al. (2017, 2018). In short, zone 1 is described by the power law parameters K_1 (consistency coefficient) and n_1 (flow index), the low shear viscosity $\eta_{0.02}$, where the subscript refers to the shear rate which the viscosity is quoted, and its end (*end of zone 1*). The transition region is characterised by the *position of the local minimum* and its relative depth ($\Delta_{\min}$). Zone 2 is again described by its onset (*start of zone 2*), the power law parameters K_2 and n_2 and the representative high shear viscosity η_{100}. Finally, also the hysteresis between the shear rate increasing and shear rate decreasing curve is described with the

positive and negative relative hysteresis H_{RS+} and H_{RS-} respectively, using the simplified calculation according to Schenker et al. (2018).

Viscoelastic properties were determined by an amplitude sweep measurement at a frequency of 0.5 Hz. The automated, strain amplitude-controlled ramp was set from 0.001 to 1000% with 60 log-equidistant distributed point measurements and automated acquisition time mode. In practice, the acquisition time was seen to be around 25.5 s for all points in all measurements. As for the flow curves, preliminary experiments have shown that the same rheograms can be obtained with different amounts of point measurements (data not shown). Here also, the descriptors introduced by Schenker et al. (2017) are evaluated, namely storage and loss moduli in the linear regime ($G'_{\max}$, $G''_{\lin}$), as well as the limit of linearity (*LoL*) and the yield stress ($\tau_{Y,\delta}$), both determined via the phase angle data. Typically, the plateau values for the storage and loss modulus in the linear viscoelastic (LVE) regime are reported. In the present and precedent work (Schenker et al. 2017) it was however found, that only the loss modulus shows this plateau characteristic, whereas the storage modulus goes through a local maximum before it decreases with increasing strain. It was therefore decided to evaluate the maximal storage modulus ($G'_{\max}$), and as commonly done, the plateau value of the loss modulus ($G''_{\lin}$). Especially at lower solids content and low strain values, the moduli data tend to be noisy, such data was omitted from evaluation. The yield point, defined by the *LoL* (or strain at yield) and the yield stress ($\tau_{Y,\delta}$)
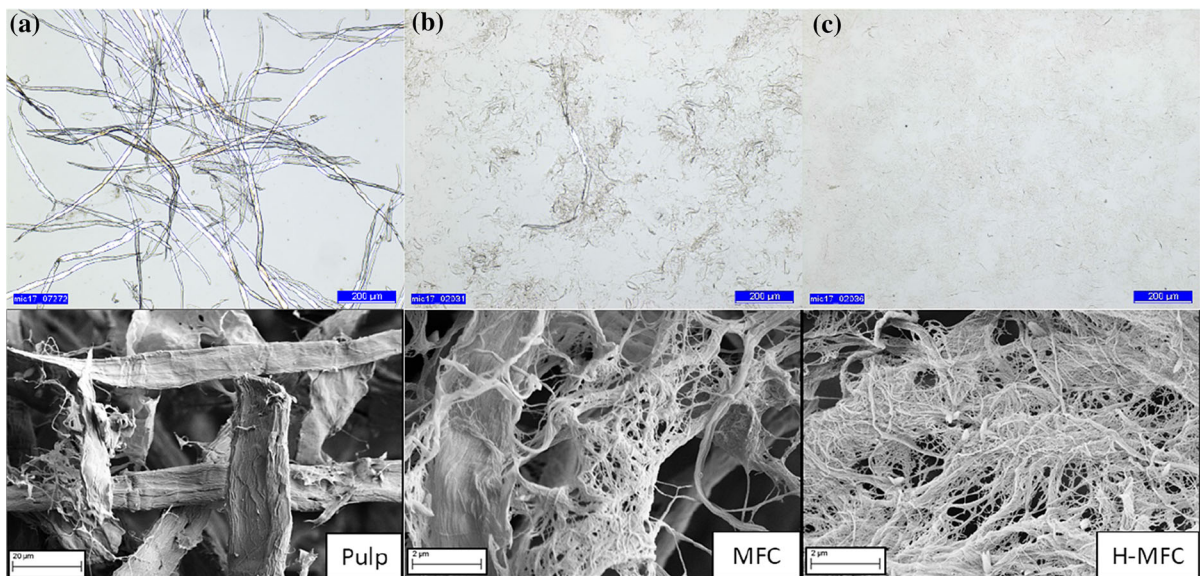
Fig. 2 Optical (top) and SEM images (bottom) of the *pulp* (**a**), *MFC* (**b**) and *H-MFC* materials (**c**). The scale bars in the optical microscopy images are 200 μm

Table 1 Specific surface area data of the *pulp*, *MFC* and *H-MFC* materials, including the standard deviations for the *MFC* and *H-MFC* materials

Material	BET surface area ($m^2\ g^{-1}$)
Pulp	0.4[a]
MFC	7.7 ± 1.1
H-MFC	19.6 ± 1.2

[a] Only one valid measurement was obtained for the *pulp* material, hence no standard deviation is provided

was determined using the phase angle data, rather than the storage modulus data (Schenker et al. 2017). As a consequence of the behaviour of the moduli as a function of strain, the phase angle typically shows a local minimum. The yield point was defined to be where the phase angle deviates (increases) more than 5% from its minimal value, adapted from Moberg and Rigdahl (2012) and further described by Schenker et al. (2017).

Results

Degree of fibrillation

The increase of the DoF from the *pulp*, through the *MFC* and to the *H-MFC* materials is apparent from the microscopy images (Fig. 2). On the one hand, the amount of clearly visible fibres and fibrils in the optical microscopy images decreases with increasing treatment intensity. On the other hand, SEM images reveal an increasing amount of fine fibrils. This qualitative observation is well supported by the surface area data presented in Table 1. It is likely, that the *MFC* material has the broadest fibril width distribution among the investigated materials, as residual fibres are present as well as isolated fibrils, whereas the other two materials contain predominantly one or the other. The role of the *pulp* material in this work is to investigate the influence of residual fibres on the suspension rheology. The hypothesised (as there is no quantitative data to proof this) differences between the *MFC* and *H-MFC* materials are the absence of residual fibres in the *H-MFC* material, together with its narrower size distribution, also resulting in a smaller median width.

Suspension particulate morphology hypothesis

As described in previous publications (Schenker et al. 2017, 2018), we place our interpretations and discussions of the present rheological data in the light of findings from other researchers. In those works, flow curves very alike the ones reported here were described, and in parallel the solid phase morphology
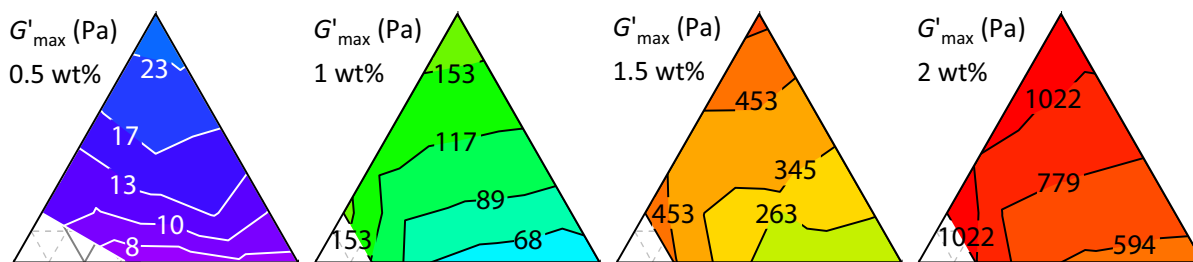
Fig. 3 Storage modulus (G'_{max}) data presented in ternary mixture contour plots for the different total solids contents of the mixtures, standard deviation was typically $\leq 10\%$. High storage modulus values are apparent for the left and top corner regions, representing high *pulp* and *H-MFC* shares respectively.

Increasing *MFC* shares at the expense of *H-MFC* and *pulp* (moving toward right corner) reduces the storage modulus. A comprehensive instruction on how to interpret the ternary diagrams can be found in the supplementary information

was visualised (Haavisto et al. 2015; Karppinen et al. 2012; Martoïa et al. 2015), confirming the aggregation behaviour in the transition region. Furthermore, a theoretical work, supported by experimental evidence, on concentrated rigid fibre suspensions containing adhesive contacts (Bounoua et al. 2016) describes the present flow curves and trends very well.

Influence of DoF on static structure morphology

Figure 3 shows the storage modulus (G'_{max}) data of the investigated mixtures. The strong dependence on the solids content is very apparent and is expected and well reported (Jia et al. 2014; Pääkkö et al. 2007; Shafiei-Sabet et al. 2012). Among the different dilutions, a very alike trend is observed. The storage modulus is highest at 100 wt% *H-MFC*, but also as high or only slightly reduced at increased *pulp* shares along and close to the 0 wt% *MFC* line. Furthermore, it increases monotonically from *MFC* to *H-MFC*. The loss modulus G''_{lin} follows the same trends (data not shown) and was lower by about one order of magnitude for all conditions. An increase of G'_{max} with an increasing DoF is expected and is reported frequently (Moberg and Rigdahl 2012; Shafiei-Sabet et al. 2016; Taheri and Samyn 2016), so the trends seen for *MFC* to *H-MFC* are expected as well. Yet, there is also work showing different trends, e.g. Shogren et al. (2011) found a maximum of moduli (and viscosity) in dependence of the amount of homogeniser passes for a corn cob based cellulose gel, or work by Saarinen et al. (2009) showed a constant decrease of G' with increasing number of passes through a fluidiser. Nechyporchuk et al. (2016b) discussed these discrepancies recently with a view on the used measurement

geometries and procedures and related the opposing trends to potential measurement artefacts and pretreatment protocols. The measurement system and procedures used in this work are in line with the recommendations to obtain reliable data given by the cited authors. The present data indicate that coarse residual fibres can have a significant influence on the storage modulus of an MFC suspension by providing a high modulus that is also observed for highly fibrillated MFCs. This previously unreported finding may be useful to consider when comparing MFC suspensions that are manufactured with different processes, as they may lead to different polydispersities and/or residual fibre contents.

The storage modulus is a measure that describes a system's ability to store elastic energy, and its increase with an increasing DoF is typically reasoned to be caused by a stronger, more homogeneous network due to the reduced fibril size (Moberg and Rigdahl 2012; Shafiei-Sabet et al. 2016). So, the observed modulus increasing effect of the *pulp* fibres is somewhat contradictory, as a more open, less connected network is present. A potential explanation may be found by considering the flexibility of the network elements, and not only the inter-fibril distances. If it is assumed that thicker fibres are more rigid compared to finer fibrils (as bending stiffness scales with the feature dimensions), then it may well be that they also can contribute strongly to the overall observed storage modulus.

Influence of DoF on yielding behaviour

With increasing strain amplitude, γ, the suspensions start to yield and their behaviour begins to be

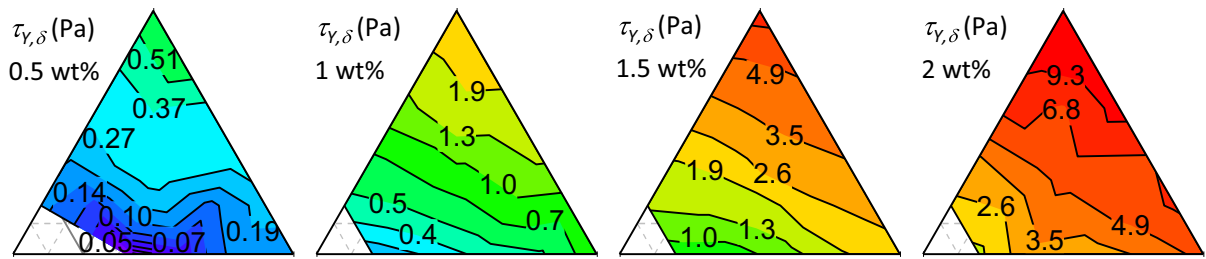**Fig. 4** Yield stress determined from the amplitude sweep measurements using the phase angle approach ($\tau_{Y,\delta}$), standard deviation was typically $\leq 5\%$. The yield stress increases with increasing DoF, i.e. low values are obtained for increased *pulp* shares (left corner), intermediate values for high *MFC* shares (right corner) and high values for high *H-MFC* shares (top corner). Exchanging shares leads to monotonically changing yield stresses
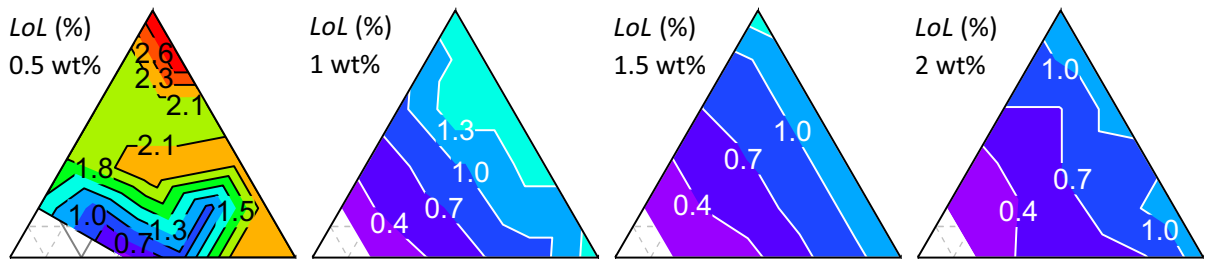

Fig. 5 Limit of linearity (*LoL*) data. For solids contents ≥ 1 wt%, the *LoL* is decreasing with an increasing *pulp* content, apparent as the contour lines are parallel to the 0 wt% *pulp* line (right triangle side). As the *LoL* was obtained from averaged amplitude sweep rheograms, no standard deviation can be calculated

determined as well by the ability of their interacting network to deform plastically (viscous dissipation). This transformation is characterised by the force (shear stress) that is needed to initiate it, and at which deformation it happens. In this work, the yield stress, $\tau_{Y,\delta}$, and the limit of linearity (*LoL*), both determined from phase angle data, δ, describe these parameters. From Fig. 4, it is apparent on the one hand, that the yield stress increases with increasing solids content [as also seen, for example, by Mohtaschemi et al. (2014a)]. On the other hand, higher DoF materials lead to increased yield stress, and residual fibres do not have an additional effect. As the yield stress will be strongly determined by the breaking of adhesive contacts and/or overcoming steric hindrances (Nechyporchuk et al. 2016b), the amount of contact points between fibrils/fibres is a determining factor for this property. The present data support this well, as increasing solids content, as well as increasing DoF (and a lower amount of residual fibres), results in a higher contact point density, and this is also supported by data from other researchers (Moberg and Rigdahl 2012; Taheri and Samyn 2016).

The corresponding limit of linearity data are presented in Fig. 5. Especially for solids contents ≥ 1 wt%, it is obvious that the *LoL* is strongly defined by the amount of residual fibres. The 0.5 wt% data show the same general trend, yet there is somewhat more variation. Furthermore, the *LoL* generally decreases with an increasing solids content, similarly to that shown in work by Jia et al. (2014). As reasoned in an earlier work (Schenker et al. 2017), this trend can be explained by a stiffening of the network with increasing solids content due to the reduction of the distance between the connection points. Using the same reasoning, residual fibres would have an opposite effect, as less connection points are present. Yet, the present data show the opposite. So, it seems more likely that the number of coarse fibres per unit component solids content is less than the fine fibres they accompany, and the additional rigidity of the coarse fibres is reducing static entanglement. Coarse fibre involvement in flocculation, due to the lower charge density compared with fines, if present, therefore, is too weak to generate a strong elastic structure at high deformation.
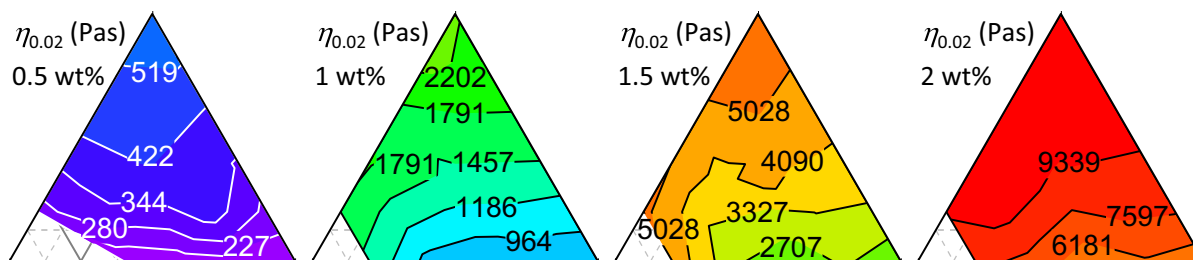
Fig. 6 Apparent low shear viscosity ($\eta_{0.02}$) data, standard deviation was typically $\leq$ 10%. The trends resemble the ones described for the storage modulus data in Fig. 3, i.e. the highest values are present at either high *pulp* (left corner) or high *H-MFC* shares (top corner)

To investigate the suspension behaviour further beyond the yield region, the constant shear experiments (flow curves) are now examined. It should be mentioned at this point, that viscosity measurements at low shear rates are very likely to be dominated by side effects. On the one hand, there is evidence for depletion near the measurement geometry boundary, leading to a water (-rich) layer (Kumar et al. 2016; Lauri et al. 2017) when smooth surfaces are used, and on the other hand, especially for larger gap settings, shear banding is likely to occur (Kumar et al. 2016; Mohtaschemi et al. 2014b). The use of serrated and/or rough surfaces or vane geometries (as in this work) are typically employed to prevent or reduce the solid depletion effects, commonly also referred to as apparent slip (Buscall 2010; Mohtaschemi et al. 2014b; Schenker et al. 2017). However, the shear banding cannot be prevented under uniform planar or axial flow, unless the measurement gap would be very small. But a small gap may lead to even more severe side effects for a heterogeneous suspension like MFC (Barnes 2000). When a critical shear stress and/or shear rate is overcome, however, the banding disappears, and so the interpretation of the results without an according correction is less critical (Martoïa et al. 2015; Mohtaschemi et al. 2014b; Servais et al. 2003). This critical shear rate or stress is very likely depending on the MFC suspension properties, but is also likely to be in zone 1 and close to the transition region for the data presented in this work (Martoïa et al. 2015; Mohtaschemi et al. 2014b; Servais et al. 2003). As we did not apply a correction to account for the shear banding, our zone 1 data have to be understood as apparent data only, yet the relative trends are likely not to be influenced by omitting to make correction(s) (Mohtaschemi et al. 2014a).

Comparing the apparent low shear viscosity data ($\eta_{0.02}$) shown in Fig. 6 with the storage modulus data (Fig. 3) reveals striking similarities, i.e. the general increase with solids content, as well as the trend for increased values at increased *H-MFC* and *pulp* shares. Even though an evaluation of the shear thinning power law behaviour may be critical with shear banding being likely, it may be worth mentioning that the flow index n_1 was basically independent of solids content and composition, fluctuating around a value of 0.13 (data not shown). If one includes the assumption of Karppinen et al. (2012), that the reforming of new contacts within the network was fast enough to compensate the breaking induced by the shear in this region of the flow curve, one may hypothesise that the viscosity in zone 1 is determined by the network-induced elastic and viscous moduli. This could explain the likeness between the apparent low shear viscosity data with the moduli data, which is often the case in complex suspensions, yet remains purely speculative.

Influence of DoF on aggregation behaviour

When increasing the shear rate further beyond a certain point it is hypothesised that the here-used MFC suspensions start to segregate into fibril rich-regions (aggregates or strong flocs) and water rich voids between them, as described in earlier work (Schenker et al. 2017, 2018) and based on findings of, for example, Karppinen et al. (2012) and Martoïa et al. (2015). This transition region is defined here by the end of zone 1 (onset of aggregation), the position of the local (viscosity) minimum, where the aggregation is believed to be maximal, and the start of zone 2, where a homogeneous structure is reinstalled/resumed. Figure 7 shows the data for the position of the local minimum and are exemplary for the end of
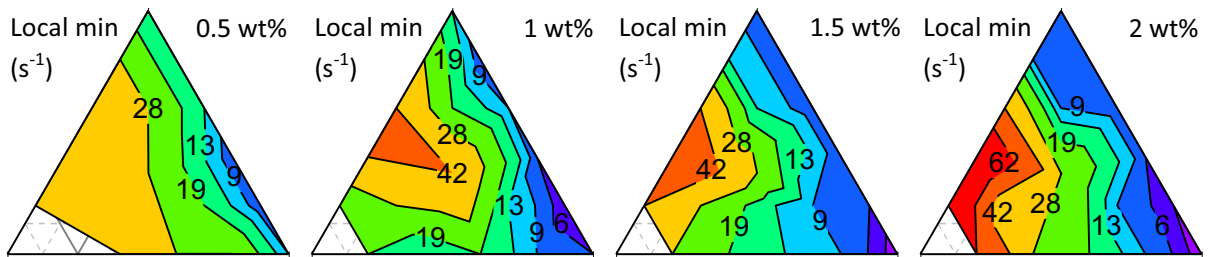
Fig. 7 Position of the local minimum data. Generally, the position of the local minimum is at lower shear rates for low *pulp* contents (right triangle side) and increases with an increasing *pulp* share (moving towards the left corner). The contour lines represent actually probed shear rate values (measurement points). As the data are discrete, no standard deviation can be provided, however, a typical variation observed was ± 1 measurement point

zone 1 as well as the start of zone 2 data, as these properties follow the same general trend. It is apparent that the position of the local minimum is shifted to higher shear rates for an increased *pulp* fibre share. The data may also indicate that the shift to higher shear rates is more pronounced for a combination of *pulp* and *H-MFC* shares. Yet, the distance from one to the next contour plot value is just one shear rate point measurement, and typically the data variation within a triplicate is ± 1 measurement point for this type of data. So, the significance between two neighbouring values may not be a given in every case. Therefore, this discussion should be considered from a more generalised point of view. Namely, the end of zone 1 (not shown), the position of the local minimum and the start of zone 2 (not shown), becomes shifted to higher shear rates, and the overall span of the transition is increased (not shown) for increased *pulp* shares. This behaviour appears to be stronger at increased solids content, though more so only when sufficient *pulp* fibres are present in the mixture. It may be hypothesised, that the coarse *pulp* fibres and/or a sufficiently high polydispersity generally hinder a structural reorganisation.

As described earlier, the relative transition zone depth (Δ_{min}) additionally characterises the degree of aggregation (Schenker et al. 2017). However, no conclusive trends with regards to the DoF were found here, yet, nonetheless, the previously found trend of increasing relative transition zone depth with decreasing solids content (Schenker et al. 2017) was reproduced (data not shown).

When a complete shear rate loop (shear rate increase ramp followed by shear rate decrease ramp) is performed, a difference between the two viscosities at a given shear rate can be seen (Fig. 1). This hysteresis was observed before and generally a difference in the suspended material morphology, caused by the respective shear history, is held responsible (Iotti et al. 2011; Martoïa et al. 2015). A recent publication by Schenker et al. (2018) discussed the potential origin of different hysteresis behaviours observed in the literature, and introduced a novel quantification approach that is applied also now in this present work. In short, two different types of hysteresis are identified: one where the viscosity of the shear rate increasing ramp is higher than the viscosity of the shear rate decreasing ramp, called positive hysteresis,
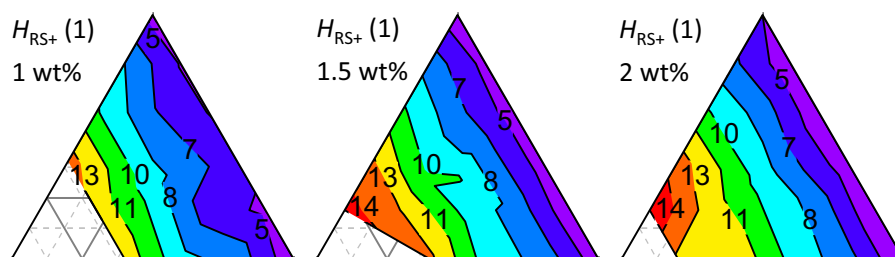

Fig. 8 Positive hysteresis data, standard deviation was typically ≤ 15%. The decrease of the positive hysteresis with a decreasing *pulp* share is apparent, as the contour lines are parallel to the 0 wt% *pulp* line (right triangle side)

and the other one, the negative hysteresis, where it is vice versa. The positive hysteresis (H_{RS+}) is attributed to the difference between the initial, homogeneous structure and the moderately aggregated structure after a full shear rate loop (Martoïa et al. 2015; Schenker et al. 2018). The negative hysteresis (H_{RS-}) appears to be mainly dominated by the viscosity drop under the level of the shear rate increasing ramp at the transition zone, and therefore related to the degree and span of aggregation during this flow curve.

Figure 8 shows the results for the positive hysteresis. Please note that the data of the 0.5 wt% suspensions (and some points of the 1 and 1.5 wt% suspensions) are not shown, because those suspensions typically showed sedimentation, starting shortly after the shear rate decrease ramp started. It is apparent that the positive hysteresis is independent of the solids content for all mixture ratios, confirming earlier findings (Schenker et al. 2018). Furthermore, there is a clear trend of higher positive hysteresis values for increased *pulp* shares. Following the above described reasoning, this may indicate a larger difference in suspension morphology between the unsheared and the pre-sheared (through the shear rate loop) state, induced by coarse fibres. It may be hypothesised again, that the coarser fibres may hinder structural rearrangements due to their stiffness compared to finer fibrils. The addition of visualisation, or other structure revealing techniques to such flow curve measurements would be of high value and could test this hypothesis. The negative hysteresis generally increases with a decreasing solids content (data not shown), that was also observed previously and attributed to a higher amount of available free water at decreased solids content (Schenker et al. 2018). Trends with the DoF are not very apparent, but a general reduction of the negative hysteresis with high *pulp* share is likely, as

well as that the highest values are typically found at a combination of 20–40% *pulp* with low to no *MFC* share. These general trends are somewhat unexpected, yet may be explained again by the stiffness of coarse fibres hindering a dense aggregate formation, for instance, (Bounoua et al. 2016), and a tendency for rather fine, easily entangling fibrils to aggregate more strongly (Naderi and Lindström 2015; Taheri and Samyn 2016). However, again, without any additional direct or indirect visualisation of the aggregated structure, such models remain hypothetical.

Influence of component mix on high shear behaviour

When the shear rate is high enough, the aggregated structure that formed in the transition region starts to break down again and the second, power law shear thinning zone starts (Bounoua et al. 2016; Karppinen et al. 2012; Martoïa et al. 2015). Here, this zone is described by the apparent high shear viscosity η_{100}, and the respective data can be found in Fig. 9. The typical increase of viscosity with solids content is clearly apparent, as well as that a higher DoF increases the high shear viscosity. This is in good agreement with the literature, consolidated in a recent review by Nechyporchuk et al. (2016b). It may be worthwhile to recall the different trend that is observed for the low shear viscosity. This difference indicates that the suspension morphologies, defining the apparent viscosities in zone 1 and 2, are different, i.e., the morphology of the sheared suspension material in zone 1 is supported by coarse, presumably stiff, fibres, whereas the morphology at increased shear rates (zone 2) is not affected by such fibres.

Further insight can be obtained by looking at the shear thinning behavior of zone 2, i.e. by looking at the
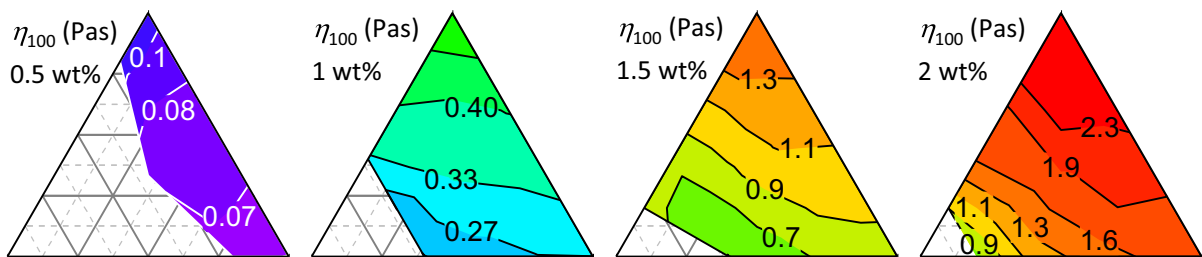

Fig. 9 High shear viscosity (η_{100}) data, standard deviation was typically ≤ 10%. The high shear viscosity generally increases monotonically with the *DoF*, i.e. it is low towards the left corner

(high *pulp* shares), intermediate towards the right corner (high *MFC* shares) and high towards the top corner (high *H-MFC* shares)
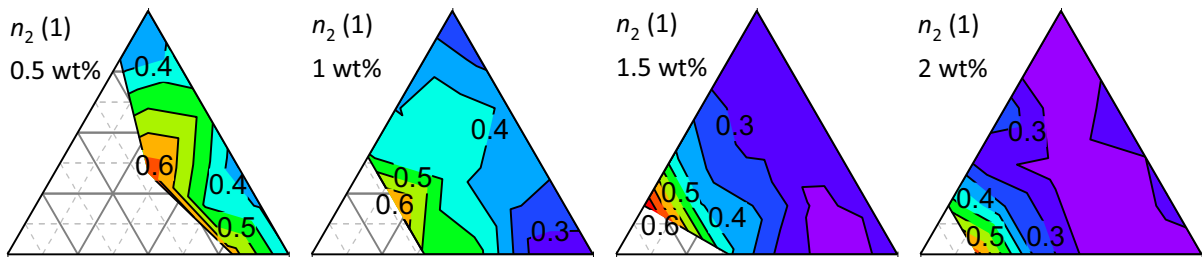
Fig. 10 Flow index of zone 2 (n_2) data, standard deviation was typically $\leq 13\%$. The general trend of n_2 appears to follow the *pulp* share, becoming higher (lesser shear thinning tendency) with an increasing *pulp* share. The maximum value is very similar for all solids content and is found at the maximal *pulp* share in the mixture

consistency coefficient K_2 and the flow index n_2. While K_2 basically shows the same trend (not shown) as the apparent high shear viscosity, the flow index appears to change strongly as a function of *pulp* content at low *pulp* contents, following also a function of solids content (Fig. 10). It should be noted also, that the flow index was the highest at the maximal possible *pulp* content before sedimentation occurred within the flow shear cycle, at each given solids content, and its absolute value was almost the same (0.64 ± 0.04) under this condition. The increase of shear thinning tendency (decrease of the flow index) with an increasing solids content was reported before for MFC suspensions (Bounoua et al. 2016; Lasseuguette et al. 2008; Schenker et al. 2017), and for pulp suspensions as well (Chaouche and Koch 2001). Bounoua et al. (2016) attributed this effect to the increasing role of attractive interactions at increased solids contents. Likewise, we (Schenker et al. 2017) attributed this effect to the increased importance of entanglements at lower shear rates of zone 2 for increased solids content. Extending those hypotheses may also explain the observed effect of a reduced shear thinning behaviour with an increased *pulp* share. As the coarser fibres lead to less entanglements and/or less attractive interactions (compared to the same mass/volume of fine fibrils), their presence resembles the effect of an increased dilution.

Conclusions

The present work investigates the rheological behaviour of suspensions containing MFC suspensions of different *DoF*s, as well as *pulp* fibres that mimic residual, unfibrillated fibres. The results follow the well-known properties of multimodal (and polydisperse) dispersions of particles in general, i.e. interactions at a distance and upon close approach (colloidal) are important flow controlling factors. The exception here is the extra factor that the fibrils are flexible to varying degree and become entangled, whereas round colloidal particles do not.

Given the above conclusion, refinements can be made in the way the flow response of complex shaped solids can be parameterised, including particle properties such as flexibility and entangled aggregate formation. It appears that the present set of data enable us to split the structure and flow behaviour into three categories with view to the observed trends as a function of the suspension composition. The first category contains the properties that are trending with the fibre/fibril widths (*DoF*) only. The second set of properties is characterised by a discontinuous behaviour, i.e. the coarse *pulp* fibres lead to the same or alike level of property effect as the highly fibrillated *H-MFC*. The third category seems to depend mainly on the *pulp* share.

The behaviour observed in the first category applies for the following properties: yield stress ($\tau_{Y,\delta}$, Fig. 4), high shear viscosity (η_{100}, Fig. 9) and the consistency coefficient in zone 2 (K_2, not shown). In all these properties, the values are increasing with an increasing *DoF*, considering the *pulp* as being equivalent to a low *DoF* component, and are also strongly increasing with the suspension solids content. Such behaviour was described before in the literature. It is typically hypothesised that the increasing amount of fibrils (due to the increased DoF and/or the increased solids content) is responsible for the respective property increase. It is reasoned, that the relative movement between fibrils is hindered by the increased amount of physical interactions and entanglements. The present

work supports those hypotheses, also for highly polydisperse MFC suspensions.

The second category, where the *pulp* share leads to a discontinuous behaviour includes specific changes in the following paramaters: storage modulus (G'_{max}, Fig. 3), loss modulus (G''_{lin}, not shown) and the low shear viscosity ($\eta_{0.02}$, Fig. 6). As mentioned in the results section, the interpretation of the low shear viscosity may be critical, though, because of potentially dominating shear banding. The trend in this category is that the unfibrillated *pulp* fibres and the highly fibrillated *H-MFC* lead to high parameter values. Alike behaviour was reported before (even though not specifically for materials containing residual fibres), yet the observed effects were attributed either to measurement artefacts related to the measurement geometries, or inadequate sample pre-treatment. It seems justifiable to assume that those artefacts were not present in this work, so it appears that this behaviour was not observed before. It is concluded that the *pulp* fibres contribute to the network strength by their stiffness, which is a direct cause of their width, whereas highly fibrillated systems gain their network strength from an increased network density and entanglement.

The properties that mainly depend on the *pulp* share include the limit of linearity (*LoL*, Fig. 5), the positive hysteresis (H_{RS+}, Fig. 8) and probably the flow index of zone 2 (n_2, Fig. 10). The reduction of the *LoL* with an increasing *pulp* share may be explained by the combined effect of the *pulp* fibres to increase the network stiffness, but also to lead to a smaller network density (less physical interactions). In turn, the lower amount of physical interactions caused by the coarser fibres may also explain the reduced shear thinning tendencies in zone 2 for higher *pulp* shares.

The trends for the aggregation descriptors with the *DoF* are not so clear, yet it appears that the coarse *pulp* fibres also influence the aggregation behaviour in the transition region, probably caused by a reduced mobility of the fibres compared to the finer fibrils. This is at least partially supported by the positive hysteresis data. The addition of rheo-optical measurement techniques to such measurements could be very insightful and probably help to reveal the mechanisms and contributions of the individual components.

In conclusion it can be stated that (residual) coarse fibres can influence the rheological properties of MFC

suspensions, not always following trends that are typically observed for changing *DoF*s. We further conclude, that it is not only the increased width that leads to a lower network density (compared to fibrils) causing these differences, but also their increased stiffness and lower mobility. To confirm this conclusion, rheo-optical investigations could be envisaged. Additionally, the impact of a polydisperse system with improved packing and smoother transitions plays a distinct role. From an application point of view, this work also has shown that it is possible to obtain MFC suspensions with specific sets of rheological properties by combining different *DoF* MFCs and pulp fibres, potentially opening up an even wider application space.

As shown by other researchers, and summarized for instance by Nechyporchuk et al. (2016b), there seem to be two different types of fibrillated cellulose types with view on their rheological behaviour and respective suspension morphology under flow. The primary difference between the two types is the surface charge, being typically low for unmodified grades and high for chemically modified grades. The latter grades typically are relatively stable colloidal suspensions due to the increased electrostatic repulsion. As this repulsion alters e.g. the frictional interactions between the fibrils, the here-presented findings cannot be transferred ad hoc to modified fibrillated cellulose grades. Additional experimental work would be needed to check the transferability.

References

Agoda-Tandjawa G, Durand S, Berot S, Blassel C, Gaillard C, Garnier C, Doublier JL (2010) Rheological characterization of microfibrillated cellulose suspensions after freezing. Carbohydr Polym 80:677–686. https://doi.org/10.1016/j.carbpol.2009.11.045

Barnes HA (2000) Measuring the viscosity of large-particle (and flocculated) suspenions: a note on the necessary gap size of rotational viscometers. J Nonnewton Fluid Mech 94:213–217. https://doi.org/10.1016/S0377-0257(00)00162-2

Besbes I, Alila S, Boufi S (2011) Nanofibrillated cellulose from TEMPO-oxidized eucalyptus fibres: effect of the carboxyl content. Carbohydr Polym 84:975–983. https://doi.org/10.1016/j.carbpol.2010.12.052

Bounoua S, Lemaire E, Férec J, Ausias G, Kuzhir P (2016) Shear-thinning in concentrated rigid fiber suspensions: aggregation induced by adhesive interactions. J Rheol 60:1279–1300. https://doi.org/10.1122/1.4965431

Buscall R (2010) Letter to the editor: wall slip in dispersion rheometry. J Rheol 54:1177–1183. https://doi.org/10.1122/1.3495981

Chaouche M, Koch DL (2001) Rheology of non-Brownian fibres with adhesive contacts. J Rheol 42:369–382. https://doi.org/10.1122/1.1343876

Cloitre M, Bonnecaze RT (2017) A review on wall slip in high solid dispersions. Rheol Acta 56:283–305. https://doi.org/10.1007/s00397-017-1002-7

Colson J, Bauer W, Mayr M, Fischer W, Gindl-Altmutter W (2016) Morphology and rheology of cellulose nanofibrils derived from mixtures of pulp fibres and papermaking fines. Cellulose 23:2439–2448. https://doi.org/10.1007/s10570-016-0987-x

Haavisto S, Salmela J, Jäsberg A, Saarinen T, Karppinen A, Koponen A (2015) Rheological characterization of microfibrillated cellulose suspension using optical coherence tomography. Tappi J 14:291–302

Herrick FW, Casebier RL, Hamilton JK, Sandberg KR (1983) Microfibrillated cellulose: morphology and accessibility. J Appl Polym Sci 37:797–813

Hubbe MA, Tayeb P, Joyce M, Tyagi P, Kehoe M, Dimic-Misic K, Pal L (2017) Rheology of nanocellulose-rich aqueous suspensions: a review. BioResources 12:9556–9661

Iotti M, Gregersen OW, Moe S, Lenes M (2011) Rheological studies of microfibrillar cellulose water dispersions. J Polym Environ 19:137–145. https://doi.org/10.1007/s10924-010-0248-2

Jia X et al (2014) Rheological properties of an amorphous cellulose suspension. Food Hydrocoll 39:27–33. https://doi.org/10.1016/j.foodhyd.2013.12.026

Kangas H, Lahtinen P, Sneck A, Saariaho AM, Laitinen O, Hellén E (2014) Characterization of fibrillated celluloses. A short review and evaluation of characteristics with a combination of methods. Nord Pulp Pap Res J 29:129–143. https://doi.org/10.3183/NPPRJ-2014-29-01-p129-143

Karppinen A, Saarinen T, Salmela J, Laukkanen A, Nuopponen M, Seppälä J (2012) Flocculation of microfibrillated cellulose in shear flow. Cellulose 19:1807–1819. https://doi.org/10.1007/s10570-012-9766-5

Kataja M, Haavisto S, Salmela J, Lehto R, Koponen A (2017) Characterization of micro-fibrillated cellulose fiber suspension flow using multi scale velocity profile measurements. Nord Pulp Pap Res J 32:473–482. https://doi.org/10.3183/NPPRJ-2017-32-03-p473-482

Korhonen M, Mohtaschemi M, Puisto A, Illa X, Alava MJ (2017) Start-up inertia as an origin for heterogeneous flow. Phys Rev E 95:022608. https://doi.org/10.1103/PhysRevE.95.022608

Kumar V, Nazari B, Bousfield D, Toivakka M (2016) Rheology of microfibrillated cellulose suspensions in pressure-driven flow. Appl Rheol 26:43534. https://doi.org/10.3933/ApplRheol-26-43534

Lasseuguette E, Roux D, Nishiyama Y (2008) Rheological properties of microfibrillar suspension of TEMPO-oxidized pulp. Cellulose 15:425–433. https://doi.org/10.1007/s10570-007-9184-2

Lauri J, Koponen A, Haavisto S, Czajkowski J, Fabritius T (2017) Analysis of rheology and wall depletion of microfibrillated cellulose suspension using optical coherence tomography. Cellulose 24:4715–4728. https://doi.org/10.1007/s10570-017-1493-5

Martoïa F, Perge C, Dumont PJJ, Orgéas L, Fardin MA, Manneville S, Belgacem MN (2015) Heterogeneous flow kinematics of cellulose nanofibril suspensions under shear. Soft Matter 11:4742–4755. https://doi.org/10.1039/c5sm00530b

Missoum K, Belgacem MN, Bras J (2013) Nanofibrillated cellulose surface modification: a review. Materials 6:1745–1766. https://doi.org/10.3390/ma6051745

Moberg T, Rigdahl M (2012) On the viscoelastic properties of microfibrillated cellulose (MFC) suspension. Annu Trans Nord Rheol Soc 20:123–130

Moberg T et al (2017) Rheological properties of nanocellulose suspensions: effects of fibril/particle dimensions and surface characteristics. Cellulose 24:2499–2510. https://doi.org/10.1007/s10570-017-1283-0

Mohtaschemi M, Dimic-Misic K, Puisto A, Korhonen M, Maloney T, Paltakari J, Alava MJ (2014a) Rheological characterization of fibrillated cellulose suspensions via bucket vane viscosimeter. Cellulose 21:1305–1312. https://doi.org/10.1007/s10570-014-0235-1

Mohtaschemi M, Sorvari A, Puisto A, Nuopponen M, Seppälä J, Alava MJ (2014b) The vane method and kinetic modeling: shear rheology of nanofibrillated cellulose suspensions. Cellulose 21:3913–3925. https://doi.org/10.1007/s10570-014-0409-x

Naderi A, Lindström T (2015) Rheological measurements on nanofibrillated cellulose systems: a science in progress. In: Mondal MIH (ed) Cellulose and cellulose derivatives. Nova Science Publishers, Inc., Hauppauge, pp 187–202

Nazari N, Kumar V, Bousfield DW, Toivakka M (2016) Rheology of cellulose nanofibers suspensions: boundary driven flow. J Rheol 60:1151–1159. https://doi.org/10.1122/1.4960336

Nechyporchuk O, Belgacem MN, Pignon F (2014) Rheological properties of micro-/nanofibrillated cellulose suspensions: wall-slip and shear banding phenomena. Carbohydr Polym 112:432–439. https://doi.org/10.1016/j.carbpol.2014.05.092

Nechyporchuk O, Belgacem MN, Pignon F (2015) Concentration effect of TEMPO-oxidized nanofibrillated cellulose aqueous suspensions on the flow instabilities and small-angle X-ray scattering structural characterization. Cellulose 22:2197–2210. https://doi.org/10.1007/s10570-015-0640-0

Nechyporchuk O, Belgacem MN, Bras J (2016a) Production of cellulose nanofibrils: a review of recent advances. Ind Crops Prod 93:2–25. https://doi.org/10.1016/j.indcrop.2016.02.016

Nechyporchuk O, Belgacem MN, Pignon F (2016b) Current progress in rheology of cellulose nanofibril suspensions. Biomacromolecules 17:2311–2320. https://doi.org/10.1021/acs.biomac.6b00668

Onyianta AJ, Williams R (2018) The use of sedimentation for the estimation of aspect ratios of charged cellulose nanofibrils. In: Fangueiro R, Rana S (eds) Advances in natural fibre composites. Springer, Cham, pp 195–203. https://doi.org/10.1007/978-3-319-64641-1_17

Orts WJ, Godbout L, Marchessault RH, Revol J-F (1998) Enhanced ordering of liquid crystalline suspensions of cellulose microfibrils: a small angle neutron scattering study. Macromolecules 31:5717–5725. https://doi.org/10.1021/ma9711452

Pääkkö M et al (2007) Enzymatic hydrolysis combined with mechanical shearing and high-pressure homogenization for nanoscale cellulose fibrils and strong gels. Biomacromolecules 8:1934–1941. https://doi.org/10.1021/bm061215p

Puisto A, Mohtaschemi M, Alava MJ (2015) Dynamic hysteresis in the rheology of complex fluids. Phys Rev E 91:042314. https://doi.org/10.1103/PhysRevE.91.042314

Pyrgiotakis G et al (2018) Development of high throughput, high precision synthesis platforms and characterization methodologies for toxicological studies of nanocellulose. Cellulose 25:2303–2319. https://doi.org/10.1007/s10570-018-1718-2

Saarikoski E, Saarinen T, Salmela J, Seppälä J (2012) Flocculated flow of microfibrillated cellulose water suspensions: an imaging approach for characterisation of rheological behaviour. Cellulose 19:647–659. https://doi.org/10.1007/s10570-012-9661-0

Saarinen T, Lille M, Seppälä J (2009) Technical aspects on rheological characterization of microfibrillar cellulose water suspensions. Annu Trans Nord Rheol Soc 17:121–128

Schenker M, Schoelkopf J, Mangin P, Gane P (2016a) Rheological investigation of complex micro and nanofibrillated cellulose (MNFC) suspensions: discussion of flow curves and gel stability. Tappi J 15:405–416

Schenker M, Schoelkopf J, Mangin P, Gane P (2016b) Rheological investigation of pigmented micro-nano-fibrillated cellulose (MNFC) suspensions: discussion of flow curves. In: Tappi international conference on nanotechnology for renewable materials, Grenoble

Schenker M, Schoelkopf J, Mangin P, Gane PAC (2017) Influence of shear rheometer measurement system selection on rheological properties of microfibrillated cellulose (MFC) suspensions. Cellulose 25:961–976. https://doi.org/10.1007/s10570-017-1642-x

Schenker M, Schoelkopf J, Mangin P, Gane P (2018) Quantification of flow curve hysteresis data: a novel tool for characterising microfibrillated cellulose (MFC) suspensions. Appl Rheol 28:22945. https://doi.org/10.3933/ApplRheol-28-22945

Servais C, Ranc H, Sansonnens C, Ravji S, Romoscanu A, Burbidge A (2003) Rheological methods for multiphase materials. In: International symposium on food rheology and structure, Zürich

Shafiei-Sabet S, Hamad WY, Hatzikiriakos G (2012) Rheology of nanocrystalline cellulose aqueous suspensions. Langmuir 28:17124–17133. https://doi.org/10.1021/la303380v

Shafiei-Sabet S, Martinez M, Olson J (2016) Shear rheology of micro-fibrillar cellulose aqueous supensions. Cellulose 23:2943–2953. https://doi.org/10.1007/s10570-016-1040-9

Shogren RL, Peterson SC, Evans KO, Kenar JA (2011) Preparation and characterization of cellulose gels from corn cobs. Carbohydr Polym 86:1351–1357. https://doi.org/10.1016/j.carbpol.2011.06.035

Stenstad P, Andresen M, Steiner TB, Stenius P (2008) Chemical surface modifications of microfibrillated cellulose. Cellulose 15:35–45. https://doi.org/10.1007/s10570-007-9143-y

Taheri H, Samyn P (2016) Effect of homogenization (microfluidization) process parameters in mechanical production of micro- and nanofibrillated cellulose on its rheological and morphological properties. Cellulose 23:1221–1238. https://doi.org/10.1007/s10570-016-0866-5

Veen SJ, Versluis P, Kuijk A, Velikov KP (2015) Microstructure and rheology of microfibril-polymer networks. Soft Matter 11:8907–8912. https://doi.org/10.1039/C5SM02086G

Yoshimura A, Prud'homme RK (1988) Wall slip corrections for Couette and parallel disk viscometers. J Rheol 32:53–67. https://doi.org/10.1122/1.549963